Image Analysis by Circularly Orthogonal Moments

Hong Dai and Simon Liao
Applied Computer Science,
The University of Winnipeg Winnipeg, Manitoba, Canada, R3B 2E9, Canada

Abstract – The orthogonal moments defined in a circular domain, such as Zernike moments and pseudo-Zernike moments, have attracted attention due to their distinctive invariance properties. In this research, the accuracy analysis of Zernike and pseudo-Zernike moment functions has been conducted. Based on our numerical schemes to improve the accuracy of the circularly orthogonal moment functions, the simulation results show that the individual orders of Zernike and pseudo-Zernike moments represent image features uniquely. In particular, we discovered that the even orders of Zernike and pseudo-Zernike moments describe most of the image characteristics, while the contributions of odd orders are very limited.

Keywords – Circularly Orthogonal Moments, Zernike Moments, Pseudo-Zernike Moments, Image Analysis, Image Reconstruction.

I. INTRODUCTION

Since they were introduced by Hu [7] in 1962, moment methods have attracted considerable attention from researchers. The desirable properties of being invariant to image scaling, translation, and rotation promote the moment-based descriptors, defined in either the circle or rectangle regions, to play significant roles in the scientific fields such as image analysis and pattern recognition. For a general study of moment methods, we refer to [10] [12] [4].

Teague first introduced Zernike moments based on the basis set of orthogonal Zernike polynomials [15]. And another related set of orthogonal moments, denoted as pseudo-Zernike moments, is derived based on the basis set of pseudo-Zernike polynomials [16]. Due to several advanced fundamental properties, particularly the distinctive property of being invariant to rotations and reflections, both Zernike and pseudo-Zernike moments are widely used in several areas, such as object recognition [8][1][6], face recognition[5][14][13], and watermarking applications[18][3].

In this research, we will focus on two circularly orthogonal moment functions, namely, Zernike moments and pseudo-Zernike moments. Based on our improved numerical schemes, we conducted image reconstructions from both Zernike and pseudo-Zernike moment functions with satisfactory results. We have also investigated the individual contributions of circularly orthogonal moment functions by reconstructing images from a partial set of either Zernike or pseudo-Zernike moments. It is concluded that the lower order moments mainly contain the fundamental information, while the higher order moments preserve image details; in particular, the even orders of Zernike moments and pseudo-Zernike moments represent most of image characteristics.

In Section 2, we review the general properties of Zernike and pseudo-Zernike moments. To verify the accuracy of Zernike and pseudo-Zernike moments, we conduct the image reconstructions from both Zernike and pseudo-Zernike moments in Section 3. The investigation of the characteristics of partial sets of Zernike and pseudo-Zernike moments will be presented in Section 4. Finally, we will make our concluding remarks in Section 5.

II. ZERNIKE MOMENTS AND PSEUDO-ZERNIKE MOMENTS

A. Zernike Moments

Zernike functions, introduced by Zernike in 1934[19], are composed of a set of complex orthogonal functions with a simple rotational property over the class of square integrable functions defined over the unit disk. The Zernike function $V_{pq}(x, y)$ is defined as

$$V_{pq}(\mathrm{x, y}) = R_{pq}(\rho)\exp(\mathrm{j}q\theta), \quad \mathrm{x}^2 + y^2 \le 1, \quad (1)$$

where $\rho = \sqrt{x^2 + y^2}$ and $\theta = arctan(y/x)$.

In (1), the radial polynomial $R_{pq}(\rho)$ of Zernike function is [16]

$$R_{pq}(\rho) = \sum_{s=0}^{\frac{p-|q|}{2}} (-1)^s \frac{(p-s)!}{s!(\frac{p+|q|}{2}-s)!(\frac{p-|q|}{2}-s)!} \rho^{p-2s}, \quad (2)$$

where $p \ge |q|$ and $p - q$ is an even number. The radial polynomial $R_{pq}(\rho)$ is an orthogonal polynomial, which leads to the orthogonality relation for $\{V_{pq}(x, y)\}$ in the two-dimensional circular domain[9]

$$\iint_D V_{pq}^*(\mathrm{x, y})V_{p'q'}(\mathrm{x, y})dxdy = \frac{\pi}{p+1}\delta_{pp'}\delta_{qq'}, \quad (3)$$

where $\delta_{pp'} = 1$ if $p = p'$ and 0 otherwise.

The Zernike moment of order p with repetition q is defined as

$$A_{pq} = \iint_D f(\mathrm{x, y}) V_{pq}^*(\mathrm{x, y})dxdy, \quad (4)$$

where $*$ denotes the complex conjugate.

In digital image processing, when the analog image function $f(x,y)$ is digitized into its discrete version $f(x_i,y_j)$, the double integration in (4) needs to be approximated by summation formulas. A commonly used formula is

$$\hat{A}_{pq} = \sum_{x_i^2 + y_j^2 \le 1}\sum f(x_i, y_j) V_{pq}^*(x_i, y_j)\Delta x\Delta y, \quad (5)$$

where Δx and Δy are the sampling intervals in the x and y directions.

When the orders of the Zernike functions are lower, (5) will provide a moderate approximation of (4). However, if the orders of the Zernike functions increase, the accuracy

of (5) will decrease.

Figure 1 shows an example of the distribution of Zernike polynomial $V_{100,60}(x, y)$ within the pixel located at $(100, 36)$ of an image sized at 256×256. It is obvious that when the order of a Zernike function rises, the accuracy of using $\Delta x \Delta y$ to approximate the double integrations in (4) will decrease.
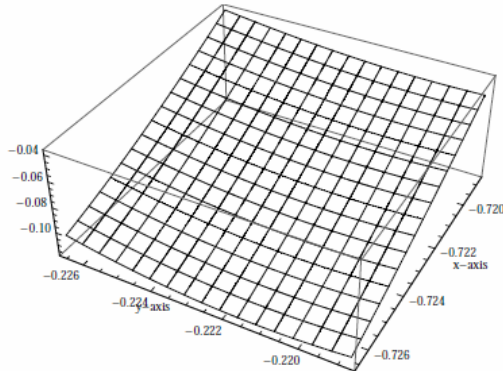

Fig.1. The distribution of Zernike polynomial $V_{100,60}(x, y)$ within the pixel located at (100, 36) of an image sized at 256×256.

Referring to the numerical scheme adopted in [17], we have applied the numerical scheme

$$\hat{A}_{pq} = \sum \sum_{x_i^2 + y_j^2 \leq 1} f(x_i, y_j) h_{pq}(x_i, y_j) \qquad (6)$$

to compute the Zernike moments in our research, where

$$h_{pq}(x_i, y_j) = \int_{x_i - \frac{\Delta x}{2}}^{x_i + \frac{\Delta x}{2}} \int_{y_j - \frac{\Delta y}{2}}^{y_j + \frac{\Delta y}{2}} V_{pq}^*(x, y) dx dy . \qquad (7)$$

By dividing a pixel into $k \times k$ sub regions with the same weights to simulate the double integrations in (7), we can increase the Zernike moment computational accuracy considerably.

Due to the completeness and orthogonality of the Zernike functions set $\{V_{pq}(x, y)\}$, we can represent an original image function $f(x, y)$ by an infinite set of its Zernike moments

$$f(x, y) = \sum_{p=0}^{\infty} \sum_{q=-p}^{q=p} \frac{p+1}{\pi} A_{pq} V_{pq}(x, y) , \qquad (8)$$

where $(p + 1)/\pi$ is the normalizing constant.

In practice, however, we can only reconstruct the original image $f(x, y)$ by a finite set of its Zernike moments approximately

$$f(x, y) = \sum_{p=0}^{T} \sum_{q=-p}^{q=p} \frac{p+1}{\pi} \hat{A}_{pq} V_{pq}(x, y) , \qquad (9)$$

where T is the truncation parameter indicating how many Zernike moments are taken into account in image reconstruction [9].

Another source of Zernike moment computation error, geometric error, is inherent and caused by using Cartesian image model for Zernike moments calculating[11]. To deal with the geometric error, we have discarded all pixels that have any sub region falling outside the unit circle in our computation process.

B. pseudo-Zernike Moments

A modified version of Zernike functions, called pseudo-Zernike function, was derived by Bhatia and Wolf in 1953[2]. It is defined as

$$V_{nm}(x, y) = R_{nm}(\rho) \exp(jq\theta), x^2 + y^2 \leq 1, \qquad (10)$$

where $\rho = \sqrt{x^2 + y^2}$ and $\theta = \arctan(y/x)$. The radial polynomials $R_{nm}(\rho)$ of pseudo-Zernike functions in (10) are different from those of Zernike functions, and are defined as

$$R_{nm}(\rho) = \sum_{s=0}^{n-|m|} (-1)^s \frac{(2n+1-s)!}{s!(n+|m|+1-s)!(n-|m|-s)!} \rho^{n-s} , \qquad (11)$$

where $n = 0, 1, 2, \ldots, \infty$, and m is restricted to $|m| < n$ only. Compared to the Zernike polynomials, the set of pseudo-Zernike polynomials contains $(n + 1)^2$ linearly independent polynomials of degree $\leq n$, while the set of Zernike polynomials contains only $(n + 1)(n + 2)/2$ linearly independent polynomials of degree $\leq n$[16].

The pseudo-Zernike moment of order n with repetition m is defined as

$$A_{nm} = \iint_D f(x, y) V_{nm}^*(x, y) dx dy . \qquad (12)$$

To compute the pseudo-Zernike moment A_{nm} in a Cartesian plane, referring to (6) and (7), we apply the formula

$$\hat{A}_{nm} = \sum \sum_{x_i^2 + y_j^2 \leq 1} f(x_i, y_j) h_{nm}(x_i, y_j) , \qquad (13)$$

where

$$h_{nm}(x_i, y_j) = \int_{x_i - \frac{\Delta x}{2}}^{x_i + \frac{\Delta x}{2}} \int_{y_i - \frac{\Delta y}{2}}^{y_i + \frac{\Delta y}{2}} V_{nm}^*(x, y) dx dy . \qquad (14)$$

We have also adopted the procedure of dividing a pixel into $k \times k$ sub regions with the same weights to simulate the double integration in (14).

Similar to the Zernike moments, we can reconstruct an original image function $f(x, y)$ from an infinite set of the pseudo-Zernike moments

$$f(x, y) = \sum_{n=0}^{\infty} \sum_{m=-n}^{m=n} \frac{n+1}{\pi} A_{nm} V_{nm}(x, y) , \qquad (15)$$

where $(n + 1)/\pi$ is the normalizing constant. In practice, we need to truncate the set of pseudo-Zernike moments to a finite number in order to reconstruct the image function $f(x, y)$

$$f(x, y) = \sum_{n=0}^{T} \sum_{m=-n}^{m=n} \frac{n+1}{\pi} \hat{A}_{nm} V_{nm}(x, y) , \qquad (16)$$

where T is the truncation parameter.

III. IMAGE RECONSTRUCTION FROM ZERNIKE MOMENTS AND PSEUDO-ZERNIKE MOMENTS

A. Image Reconstruction from Zernike Moments

To verify our newly proposed numerical schemes to compute the Zernike moments, we will conduct the image reconstruction tasks by applying (9). Figure 2 shows two

testing images utilized in this research. The image (a) is sized by 256×256 with 256 gray levels, and (b) is sized by 128×128 with 256 gray levels.
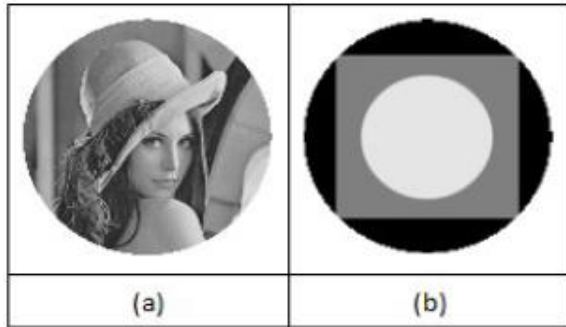

Fig.2. The testing image (a) sized by 256×256 and (b) sized by 128×128. Both of the testing images have 256 gray levels.

The Peak Signal to Noise Ratio (PSNR) is applied in our experiment as the measurement to compare the reconstructed images with the original testing image. PSNR is the ratio between the maximum power of the signal and the affecting noise and is image independent. The definition of PSNR is given by

$$PSNR = 10\log_{10}\left(\frac{MAX_I^2}{MSE}\right), \qquad (17)$$

where MAX_I is the maximum gray level value of the image, which is 255 for our testing images. The Mean Squared Error (MSE) is defined as

$$MSE = \frac{1}{N^2}\sum_{i=1}^{N}\sum_{j=1}^{N}[f(x_i, y_j) - \hat{f}(x_i, y_j)]^2, \qquad (18)$$

where $f(x_i, y_j)$ and $\hat{f}(x_i, y_j)$ are the original image and the reconstructed image, respectively.
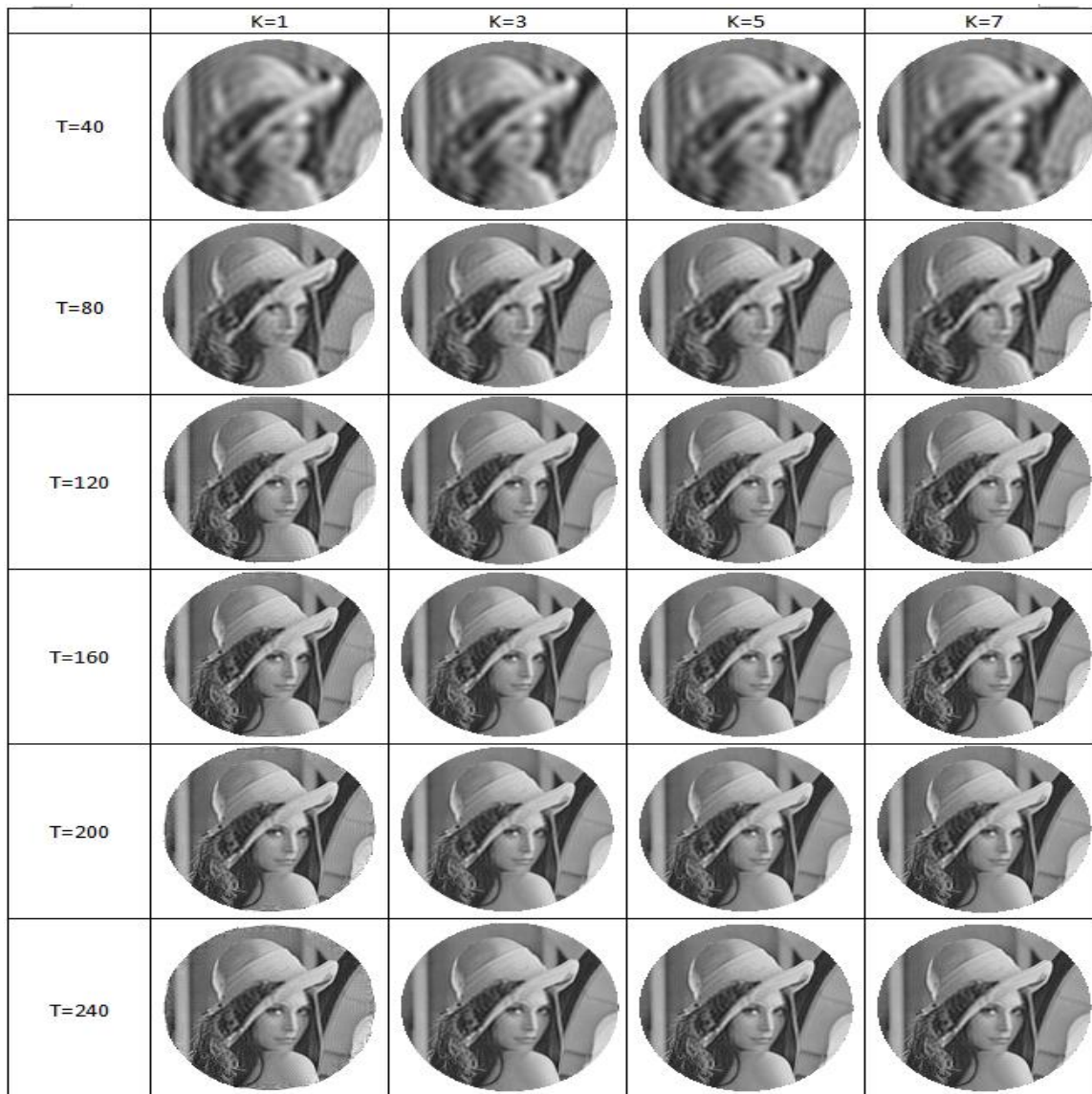
Fig.3. Some reconstructed image from different maximum Zernike moments with various $k \times k$ numerical schemes.

Figure 3 displays some reconstructed Figure 2 (a) from different maximum orders of Zernike moments with various $k \times k$ numerical schemes. The corresponding PSNR values of these reconstructed images are shown in Table 1.

Table 1: Corresponding PSNRs of Figure 3

	k=1	k=3	k=5	k=7
T=40	22.859	22.799	22.780	22.772
T=80	24.761	25.398	25.391	25.397

T=120	24.885	27.148	27.153	27.152
T=160	24.414	27.912	27.928	27.933
T=200	23.647	28.192	28.189	28.202
T=240	22.901	28.301	28.350	28.350

With the 7×7 numerical scheme, we reconstructed Figure 2 (b) from different maximum orders of Zernike moments. Figure 4 illustrates some of the reconstructed images.
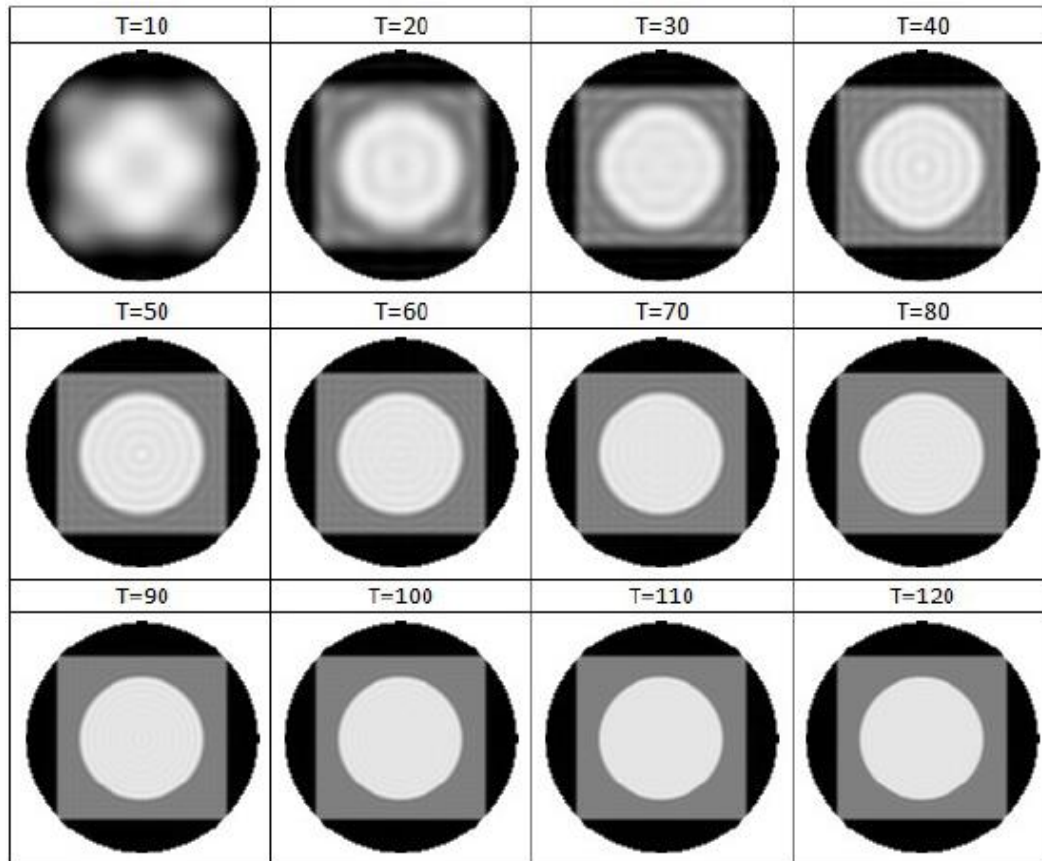
Fig.4. Some reconstructed images from different maximum orders of Zernike moments with the 7×7 numerical scheme.

B. Image Reconstruction from pseudo-Zernike Moments

We have performed the image reconstruction tasks from pseudo-Zernike moments as well. Figure 5 shows some reconstructed images from different maximum orders of pseudo-Zernike moments with various numerical schemes, while Table 2 exhibits the corresponding PSNR values of these reconstructed images shown in Figure 5.

Table 2: Corresponding PSNR values of the reconstructed images shown in Figure 5

	k=1	k=3	k=5	k=7
T=40	24.132	24.153	24.134	24.126
T=80	25.503	26.726	26.721	26.742
T=120	25.442	27.614	27.616	27.613
T=160	24.655	27.902	27.923	27.926
T=200	24.006	28.062	28.071	28.088
T=240	23.407	28.139	28.185	28.180

Figure 6 displays some reconstructed Figure 2 (b) from different maximum orders of pseudo-Zernike moments with the 7×7 numerical scheme.

With the same maximum orders and $k \times k$ numerical scheme, the reconstructed images from pseudo-Zernike moments are superior to the images reconstructed from Zernike moments. This can be explained by the set of pseudo-Zernike moments containing $(n + 1)^2$ linearly independent polynomials, while the set of Zernike polynomials holds only $(n + 1)(n + 2)/2$ linear independent polynomials. Therefore, for the same maximum order, the pseudo-Zernike moments preserve more image information than the Zernike moments.

Fig.5. Some reconstructed images from different maximum orders of pseudo-Zernike moments with various $k \times k$ numerical schemes.

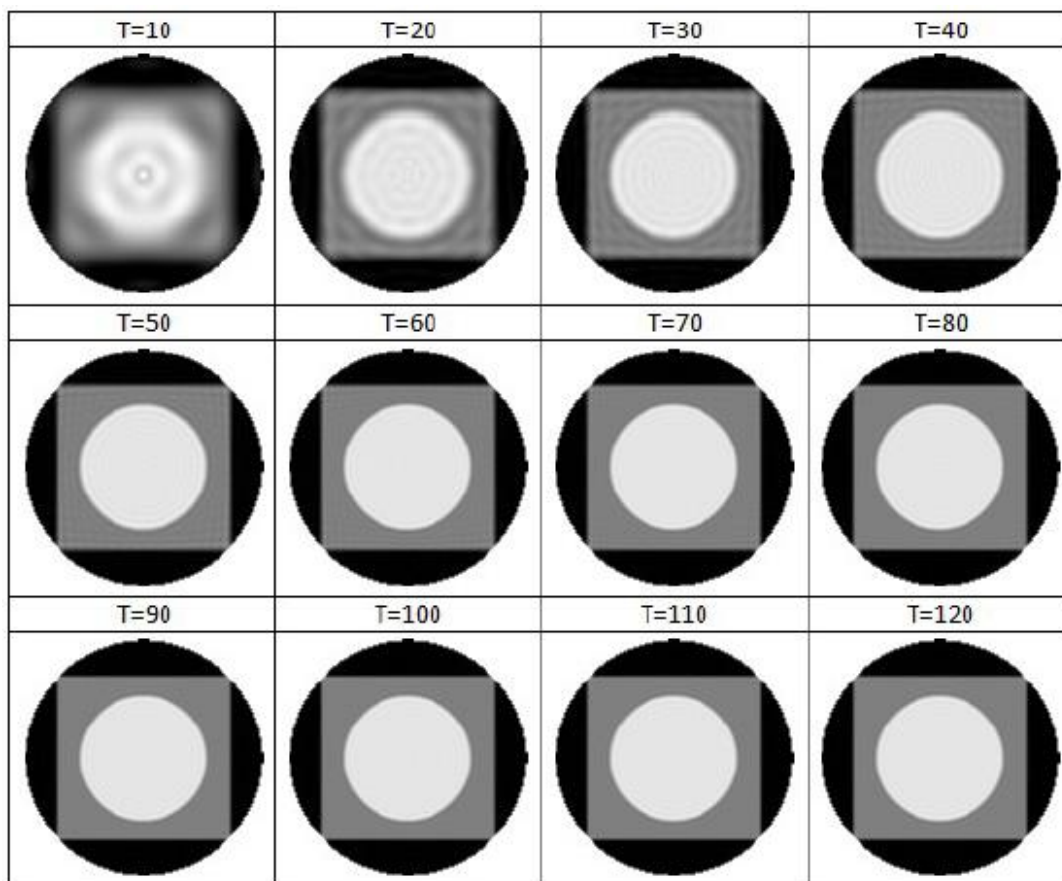Fig.6. Some reconstructed image from different maximum pseudo-Zernike moments with the 7×7 numerical scheme.

IV. IMAGE RECONSTRUCTIONS FROM PARTIAL SETS OF CIRCULARLY ORTHOGONAL MOMENTS

With the previously presented more accurate moment computation results and reconstructed images, we are able to investigate the individual contributions by a partial set of Zernike and pseudo-Zernike moment functions.

C. Image Reconstructions from Partial Sets of Zernike Moments

To inspect the image reconstruction performances determined by a limited set of Zernike moments, we adopt the formula

$$\hat{f}(x, y) = \sum_{p=T1}^{T2} \sum_{q=-p}^{q=p} \frac{p+1}{\pi} \hat{A}_{pq} V_{pq}(x, y), \ |q| \leq p \text{ and } p-q = \text{even}$$

(19)

where T1 and T2 decide the range of the partial sets of Zernike moments.
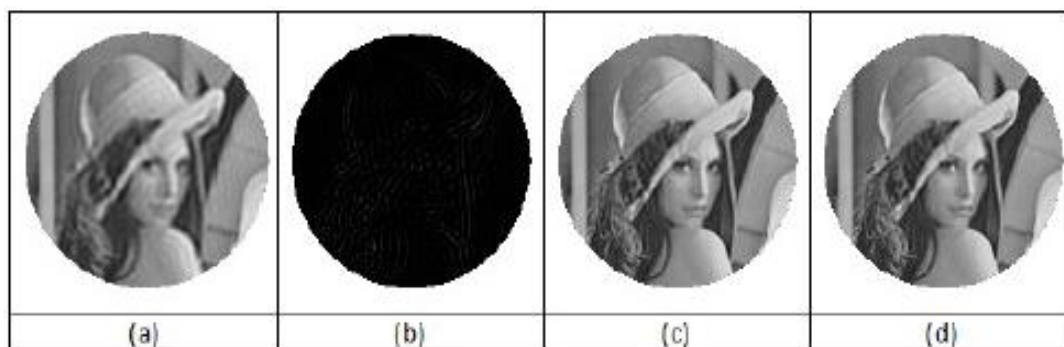
Fig.7. (a) Image reconstructed by the orderset of 0 to 80; (b) Imagereconstructed by the order set of 81 to 240; (c) Image reconstructed by the order set of 0 to 240; (d) Image obtained by performing the direct additional operation on (a) and (b).

Figure 7 shows the reconstructed Figure 2 (a) from the sets of Zernike moments orders 0 to 80, 81 to 240, 0 to 240, and the image obtained by the direct addition operation of the sub-figures Figure 7 (a) and (b). It should be noted that Figure 7 (c) and (d) are identical, which indicates that the contributions of individual sets of

Zernike moments in the image reconstruction process are independent and accumulative. It is obvious that the lower order sets of Zernike moments contain more fundamental image information, while thehigher order sets of Zernike moments represent more image details.

To address the characteristics of partial sets of Zernike moments further,we have conducted the image reconstructions from either the even or oddorders of Zernike moment functions only. According to the definition of Zernike functions, the integer q takes positive, negative, or zero values, and satisfies

$$|q| \leq p$$

where $p - |q|$ is an even number. Therefore, to investigate the characteristics of either even or odd order sets of Zernike moments, we only need to consider parameter p.

Table 3 illustrates the details of choosing the parameter p for image reconstructions by either the odd or even order sets of Zernike moment functions only. The odd order sets are highlighted in blue, while the even order sets of Zernike moments are highlighted in gold.

Table 3: The structure of using order p to reconstruct an image

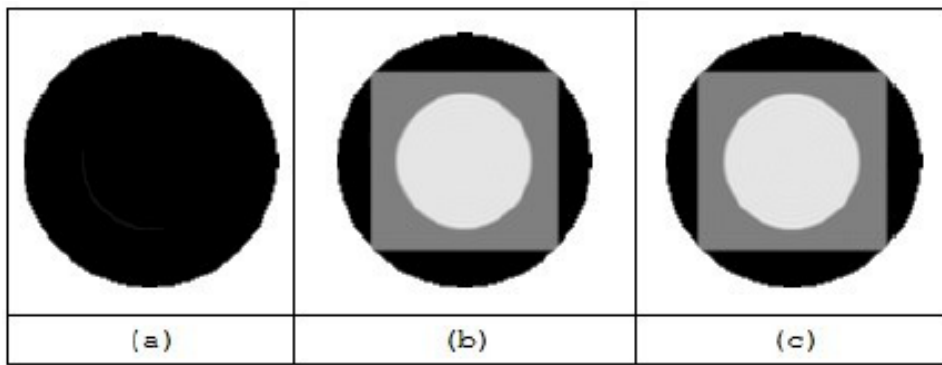|					Z_{00}					
				$Z_{1,-1}$		Z_{11}				
			$Z_{2,-2}$		Z_{20}		Z_{22}			
		$Z_{3,-3}$		$Z_{3,-1}$		Z_{31}		Z_{33}		
	$Z_{4,-4}$		$Z_{4,-2}$		Z_{40}		Z_{42}		Z_{44}	
$Z_{5,-5}$		$Z_{5,-3}$		$Z_{5,-1}$		Z_{51}		Z_{53}		Z_{55}

Fig.8. (a) Image reconstructed by the odd order set; (b) Image reconstructed by the even order set; (c) Image reconstructed by the complete order set of Zernike moments.
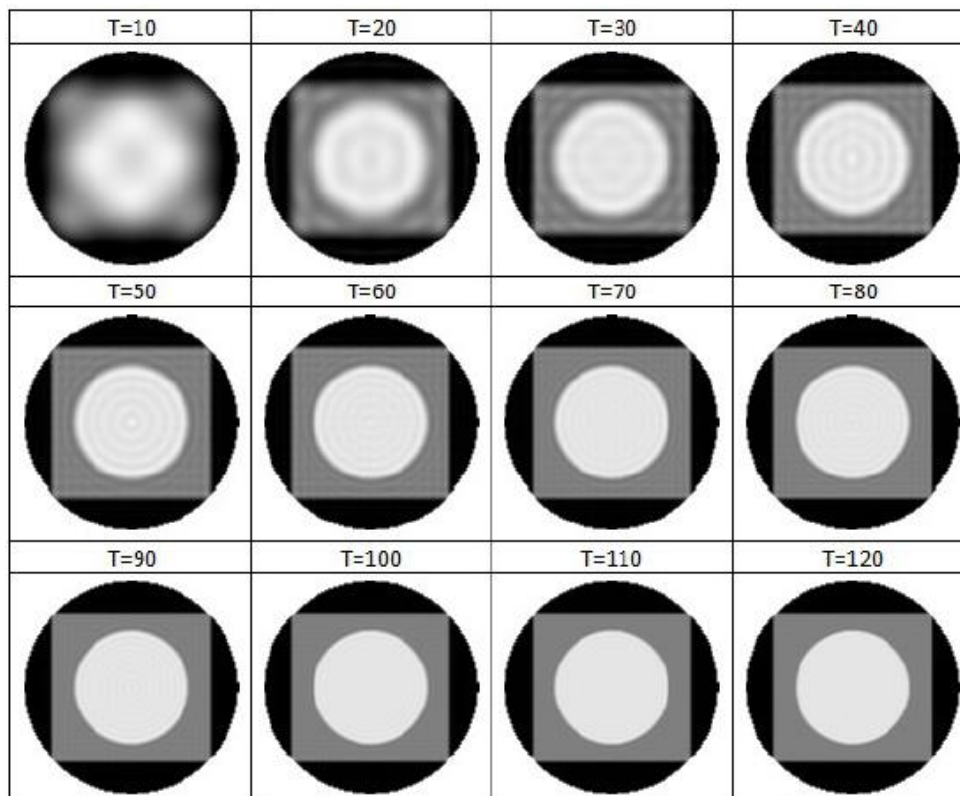

Fig.9. Image reconstructed from different even order sets of Zernike moments with the7×7 numerical scheme on Figure 2 (b).

Figure 8 shows the reconstructed images of Figure 2 (b) from the Zernike moments by using the odd order sets of 1 to 119, the even order sets of 0 to 120, and the complete sets of 0 to 120, respectively. It can be clearly observed that the set of even orders of Zernike moments contributes nearly all of the image characteristics of the original image, while the image representation of the odd order of Zernike moments is very limited.
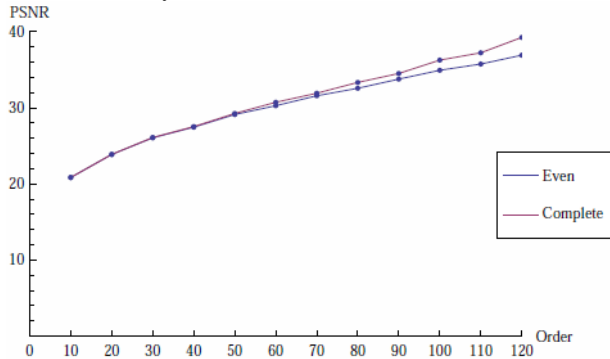

Fig.10. PSNRs comparison of the reconstructed images presented in Figure 4 and Figure 9.

Figure 9 presents some reconstructed Figure 2 (b) from different even order sets of Zernike moment functions. Compared with the image reconstruction performances shown in Figure 4, the visual differences between the two sets of reconstructed images are ignorable. Figure 10 displays the PSNR values of the reconstructed images presented in both Figure 4 and Figure 9 for comparison.

D. Image Reconstructions from Partial Sets of pseudo-Zernike Moments

To investigate the image reconstruction performances from a limited set of pseudo-Zernike moments, we utilize the formula

$$\hat{f}(x, y) = \sum_{n=T1}^{T2} \sum_{m=-n}^{m=n} \frac{n+1}{\pi} \hat{A}_{nm} V_{nm}(x, y), \quad |m| \le n, \text{(20)}$$

where T1 and T2 indicate the upper and lower bounds of the partial sets of pseudo-Zernike moments.

Figure 11 displays the images reconstructed from Figure 2 (a) with two partial sets of pseudo-Zernike moments, orders ranged from 0 to 80 and 81 to 240, the completed set of pseudo-Zernike moments orders from 0 to 240, and the image achieved by the direct addition operation on (a) and (b). As expected, Figure 11 (c) and (d) are identical because individual sets of pseudo-Zernike moments contribute in the image reconstruction process independently. Similar to the Zernike moments, the lower order sets of pseudo-Zernike moment functions represent more fundamental image information, whilethe higher order sets include more details.
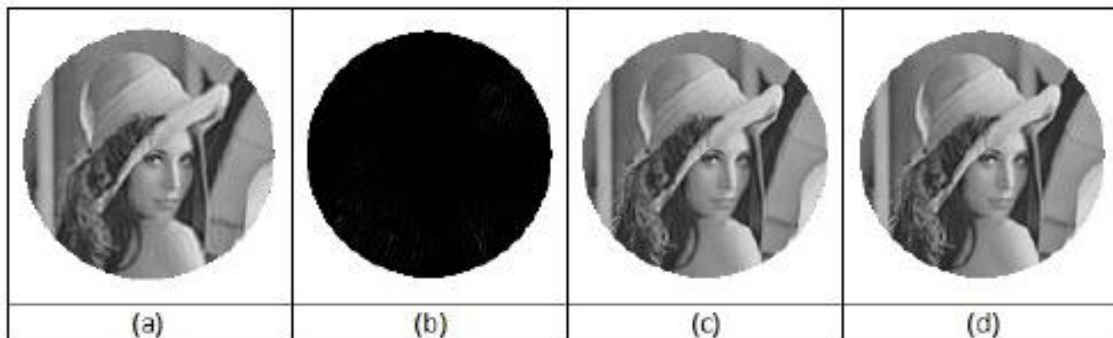

Fig.11. (a) Image reconstructed by the order set of 0 to 80; (b) Image reconstructed by the order set of 81 to 240; (c) Image reconstructed by the order set of 0 to 240; (d) Image resulted by performing the additional operation on (a) and (b) directly.

In this research, we have also performed the image reconstruction tasks using only the even or odd orders of pseudo-Zernike moment functions.

Table 4: The structure of using order m to reconstruct an image.

By the definition of pseudo-Zernike functions, the only limitation of m is $|m| < n$. Table 4 demonstrates the parity of the parameter m of pseudo-Zernike functions. The columns highlighted by gold represent the even order sets of pseudo-Zernike functions, while the odd order sets are highlighted by blue.

Figure 12 presents the reconstructed Figure 2 (b) from the pseudo-Zernike moment functions with the set of odd orders 1 to 119, the set of even orders 0 to 120, and the complete set of pseudo-Zernike moments of orders 0 to 120, respectively. Similar to the image reconstructions using the Zernike moment functions, the even order sets of pseudo-Zernike moments provide most of the image descriptions of the original image, while the image information represented by the odd order sets is very lacking.

Figure 13 displays some reconstructed images of Figure 2 (b) from different even order sets of Zernike moment functions. We can observe that the visual differences between the two collections of the reconstructed images in

Figure 4 and Figure 9 are very limited. For comparison, Figure 14 shows the PSNR values of the reconstructed images presented in both of Figure 4 and Figure 9.
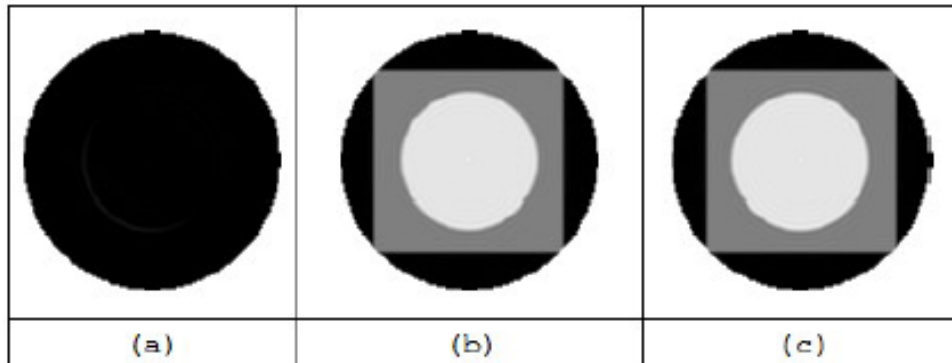

Fig.12. (a) Image reconstructed by the set of odd order pseudo-Zernike moments; (b) Imagereconstructed by the set of even order pseudo-Zernike moments; (c) Imagereconstructed by the complete set ofpseudo-Zernike moments.
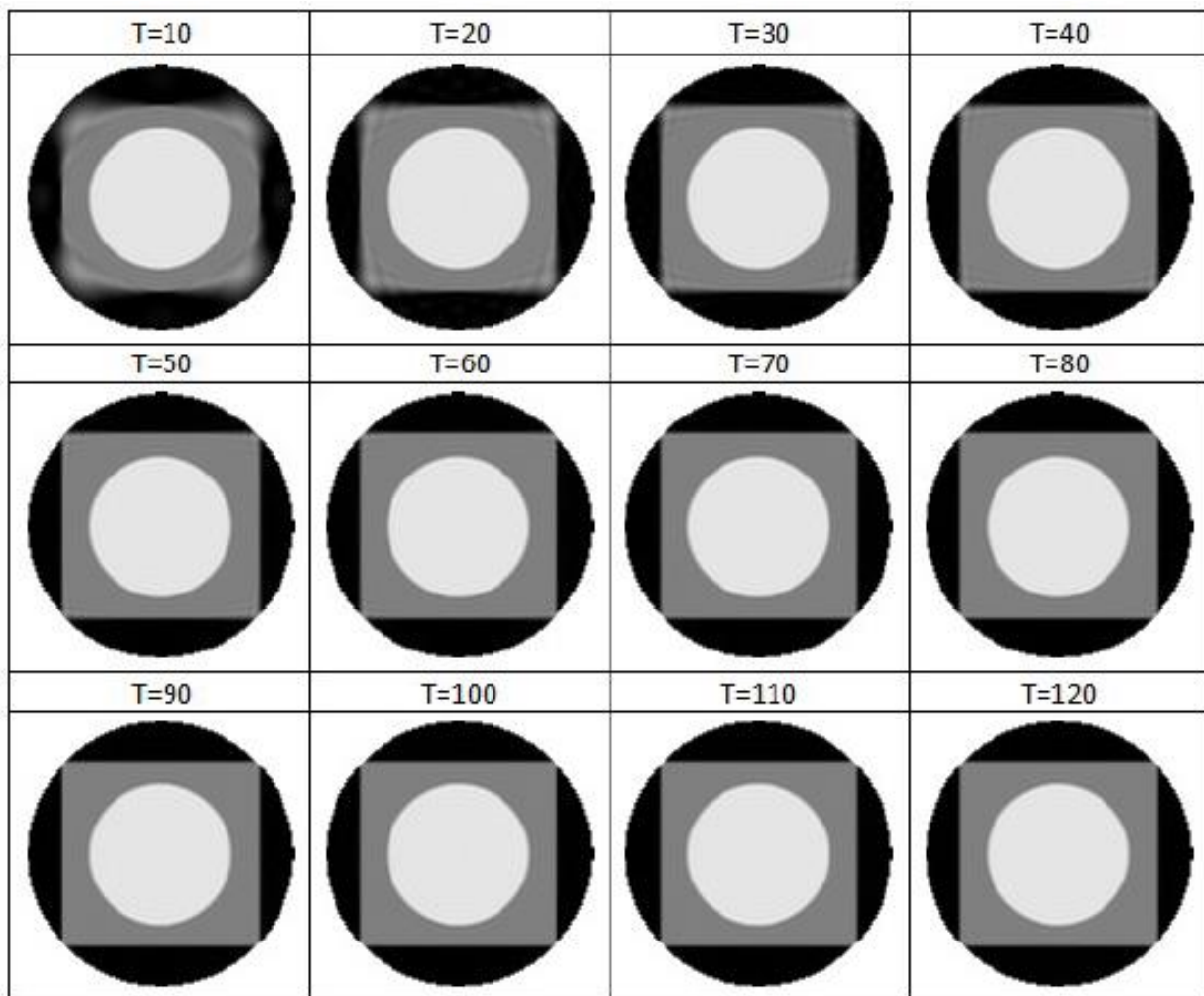

Fig.13. Images reconstructed from different even order setsof pseudo-Zernike moments with the 7×7 numerical scheme.
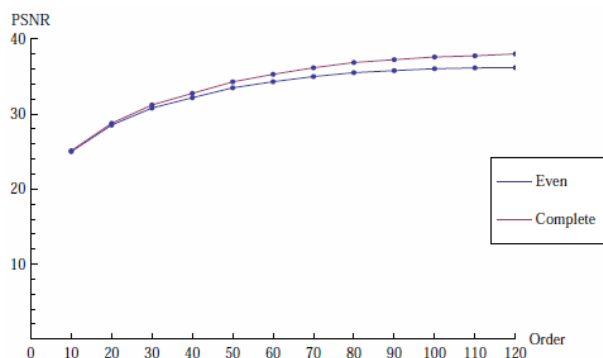
Fig.14. PSNRs comparison of the reconstructed images presented in Figure 6 and Figure 13.

V. CONCLUDING REMARKS

In this research, we have conducted the accuracy analysis of orthogonal moment functions defined in a circular domain and proposed a numerical scheme to improve calculations of the circularly orthogonal moment functions. To verify the validity of this numerical method, we have performed the image reconstructions from higher orders of Zernike and pseudo-Zernike moment functions with satisfactory results.

We have investigated the image reconstructions from partial sets of Zernike and pseudo-Zernike moment functions as well. Our experimental results are inline with the general moment theory that the lower orders moment functions contain most of the fundamental information of the original image, while the higher orders moments represent more detailed image features. Furthermore, we have discovered that the even order sets of Zernike moments and pseudo-Zernike moments characterize most of the image characteristics, while the contributions of the odd order sets are very limited.

REFERENCES

[1] Erol A. Nicolescu M. Amayeh G., Bebis G. Peg-free hand shape verification using high order zernike moments. *IEEE*, page 40, 2006.
[2] AB Bhatia and E Wolf. On the circle polynomials of zernike and relatedorthogonal sets. *Proc. Cambridge Philos. Soc*, 50:40-48, 1954.
[3] Shirani S. Farzam M. A robust multimedia watermarking technique using zernike transform. *IEEE*, pages 529{534, 2001.
[4] J. Flusser, T. Suk, and B. Zitova. *Moments and moment invariants in pattern recognition*. John Wiley & Sons, Ltd, 2009.
[5] Faez K. Hadadnia J. and Ahmadi M. An efficient human face recognition system using pseudo zernike moment invariant and radial basis function neural network. Int. J. Patt. Recogn. Artif. Intell., 17, 2003.
[6] Newton A.R. Hse H. Sketched symbol recognition using zernike moments. *IEEE*, 1:367-370, 2004.
[7] M. K. Hu. Visual pattern recognition by moment invariants. *IRE Transactions on Information Theory*, 8:179-187, 1962.
[8] Yaw Hua Hong Khotanzad A. Invariant image recognition by Zernike moments. *IEEE*, 12(5):489-497, 1990.
[9] S. Liao and M. Pawlak. On the accuracy of zernike moments for image analysis. *IEEE transactions on pattern analysis and machine intelligence*, 20(12):1358-1364, 1998.

[10] R. Mukundan and K.R. Ramakrishnan. *Moment Functions in Image Analysis - Theory and Applications*. World Scienti_c, 1998.
[11] M. Pawlak and S. Liao. On the recovery of a funtion on a circulardomain. IEEE transaction on information theory, 48(10):2736-2753,2002.
[12] MiroslawPawlak. *Image Analysis by Moments: Reconstrcution and Aomputational Aspects*. Oficyna Wydawnicza Politechniki Wroc Lawskiej, WrocLaw, 2006.
[13] C Singh, E Walia, and N Mittal. Rotation invariant complex Zernike moments features and their applications to human face and characterrecognition. *IET computer vision*, 5(5):255-266, 2011.
[14] Chandan Singh, Neerja Mittal, and EktaWalia. Face recognition usingzernike and complex zernike moment features. *Pattern Recognition and Image Analysis*, 21(1):71-81, 2011.
[15] M. R. Teague. Image analysis via the general theory of moments. *Opt*.Soc. Am., 70:920-930, 1980.
[16] C. H. Teh and R. T. Chin. On image analysis by the methods of moments. *IEEE transactions on pattern analysis and machine intelligence,*10(4):496-513, 1988.
[17] Xiaoyu Wang and Simon Liao. Image reconstruction from orthogonalfourier-mellin moments. Image Analysis and Recognition, pages 687-694,2013.
[18] Pawlak M. Yongqing Xin, Liao S. A multibit geometrically robust imagewatermark based on zernike moments. IEEE, 4:861-864, 2004.
[19] von F Zernike. Beugungstheorie des schneidenver-fahrens und seinerverbesserten form, der phasenkontrastmethode. Physica, 1(7):689-704, 1934.